



Hall-Effect-Modulated Thermal Transport Enhancement in Hybrid Nanofluid Flow over a Stretching Surface Using Taguchi Optimization



Ram Prakash Sharma^{1*}, Bimal Kumar Barik², Sriram Praharaj², V. Vinay Kumar², Abhishek Sharma²

¹ Department of Mechanical Engineering, National Institute of Technology Arunachal Pradesh, 791113 Itanagar, India

² Department of Basic & Applied Science, National Institute of Technology Arunachal Pradesh, 791113 Itanagar, India

* Correspondence: Ram Prakash Sharma (ramprakash0808@gmail.com)

Received: 01-15-2026

Revised: 03-07-2026

Accepted: 03-22-2026

Citation: R. P. Sharma, B. K. Barik, S. Praharaj, V. V. Kumar, and A. Sharma, "Hall-effect-modulated thermal transport enhancement in hybrid nanofluid flow over a stretching surface using Taguchi optimization," *J. Complex Multiphys. Eng. Syst.*, vol. 1, no. 1, pp. 82–97, 2026. <https://doi.org/10.56578/jcmes010105>.



© 2026 by the author(s). Licensee Acadlore Publishing Services Limited, Hong Kong. This article can be downloaded for free, and reused and quoted with a citation of the original published version, under the CC BY 4.0 license.

Abstract: Efficient thermal management in electrically conducting fluids is critically required in advanced engineering systems, including power generation, electronic cooling, and nuclear reactor technologies, where strong magnetic fields significantly influence transport phenomena. In the present study, steady, incompressible flow of a hybrid nanofluid over a porous stretching surface was systematically investigated under the combined effects of Hall current, thermal radiation, and a spatially varying heat source. The hybrid nanofluid was formulated by dispersing tricalcium phosphate ($\text{Ca}_3(\text{PO}_4)_2$) and molybdenum disulfide (MoS_2) nanoparticles in water. The governing nonlinear partial differential equations were transformed into a system of coupled ordinary differential equations through similarity transformations, and numerical solutions were obtained using a fourth-order Runge–Kutta method coupled with a shooting algorithm. To further optimize the thermal transport characteristics, the Taguchi optimization technique with an L_{16} orthogonal array was employed to evaluate the relative significance of key parameters and to identify optimal parametric combinations. The results reveal that the hybrid nanofluid exhibits superior thermal performance compared with conventional nanofluids. These findings provide valuable insights for the design and optimization of multiphysics thermal systems involving magnetohydrodynamic flows and hybrid nanofluids, thereby contributing to the development of high-efficiency thermal management technologies.

Keywords: Hybrid nanofluid; Hall current; Thermal radiation; Taguchi optimization; Heat transfer enhancement

1 Introduction

In an era of rising energy demands, hybrid nanofluids have become a groundbreaking development in thermal engineering. They provide high thermal conductivity and heat transfer by synergistically combining more than one nanoparticle in a base fluid. Their revolutionary applications include solar energy systems, aerospace cooling, microelectronics, biomedical therapeutics and industrial heat exchangers, pushing the frontiers of contemporary thermal management in multiphysics engineering systems. As a result, the scientific community has seen a phenomenal increase in research interest in hybrid nanofluids, which they have realized as a necessary pillar of future energy-efficient technologies. Sharma et al. [1] focused on magnetohydrodynamic flow of hybrid nanofluid through a damaged artery using a numerical method-based solver. They showed the impact of nanoparticles on wall shear stress, velocity, and impedance, which could be of use in drug delivery systems and biomedical applications. The thermosolutal Marangoni stagnation hybrid nanofluid flow hybrid nanofluid across an extending sheet was demonstrated by Mohanty et al. [2]. The research by Manimegalai and Kameswaran [3] on the hybrid nanofluid flow in solar collectors indicated that radiation, magnetic field, and amount of nanoparticles influence the heat transmission, enhancing thermal conduction. Parida et al. [4] studied a magnetohydrodynamic flow of hybrid nanofluid containing gold and multiwalled carbon nanotubes in blood. It was found that thermal radiation raises temperature while magnetic fields reduce the velocity. Various studies [5–7] analyzed the hybrid nanofluid flow past a different geometry considering the effects of magnetic fields with thermal effects such as radiation, dissipative heat, and internal heat generation.

A magnetic field is employed perpendicular to an electrically conducting fluid and charge carriers are deflected sideways, leading to a transverse current, which causes a Hall current. The phenomenon is critical to modern applications in electromagnetic engineering since it has a substantial influence on the velocity distribution and thermal transfer behavior in magnetohydrodynamic flows. Rana et al. [8] studied the flow of nanofluids over a revolving disk, considering the effects of Hall current and nanoparticle aggregation using the finite difference method. Hakeem et al. [9] studied the hybrid nanofluid flow over a spinning cone. They numerically solved the governing equations using the Runge-Kutta shooting method. Kanimozhi et al. [10] investigated mixed convective Jeffrey fluid flow across an oblique upright plate. The perturbation approach was used to solve the problem analytically. Many investigations [11–14] incorporated the influence of magnetic fields and Hall currents in a variety of geometries using porous media.

Thermal radiation can be described as the emission of electromagnetic waves that are produced exclusively by the thermal movements of particles in a body. This radiative mechanism of heat transfer becomes more and more dominant at high temperatures, having a significant effect on the temperature of fluids and becoming an extremely important consideration in the analysis of heat transfer in fluids. Banakar et al. [15] investigated radiative nanofluid flow over an off centric disk considering micro inertial effect. Madhukesh et al. [16] used the Runge–Kutta–Fehlberg method to obtain numerical solutions of nanofluid flow over a Riga surface in a porous material, focusing on radiation and nanoparticle aggregation. The results showed that porosity reduces fluid velocity, whereas aggregation enhances heat dispersion. A numerically analyzed Maxwell hybrid nanofluid flow over a porous stretching plate was discussed by Jayaprakash et al. [17] They revealed that magnetic flux and thermal radiation significantly influence heat transfer, while nanoparticle shape strongly affects temperature, concentration, and flow behavior. Furthermore, several researchers [18–21] considered the impact of thermal radiation in hybrid nanofluid flows through various geometries such as microchannels, porous Riga surfaces, stretching sheets, and spinning disks. Ramadevi et al. [22] illustrated the magnetohydrodynamic Carreau fluid flow over a widening surface with the emphasis on the effects of dissipative heat and a variable heat source. It was demonstrated that non-uniform sources significantly influence the dynamics of thermal and mass transport. Govindarajulu et al. [23] investigated the magnetohydrodynamic hybrid nanofluid flow through an upright channel with the influence of a non-uniform heat source using a numerical method. Madhukesh et al. [24] applied the Runge–Kutta method to address the governing equations of hybrid nanofluid flow in a microchannel with the effects of waste discharge and space- and time-dependent heat sources. In addition, several recent studies [25–28] investigated the behavior of thermal transfer in hybrid nanofluid flows over Riga surfaces, extending sheets, and tubes, with the effects of non-uniform heat sources.

Genichi Taguchi created the reliable statistical technique known as Taguchi optimization to methodically determine the ideal process parameters with the fewest possible experimental trials. It effectively reduces variability and increases performance output by utilizing orthogonal arrays and signal-to-noise ratio analysis, making it a very potent instrument in contemporary engineering and thermal research optimization. By optimizing discrete V-down baffle settings in a solar air heater using the Taguchi–Technique for Order of Preference by Similarity to Ideal Solution (TOPSIS) approach, Sharma et al. [29] improved thermo-hydraulic performance and heat transfer efficiency through Taguchi design analysis. Kumar et al. [30] studied the blood flow of gold and zinc nanoparticles in an inclined microchannel. To optimize entropy formation under radiation and heat source impacts, they used Taguchi and ANOVA techniques. Cicek and Johnson [31] used Taguchi and Gray relational analysis to study polycarbonate three-dimensional printing parameters in order to maximize tensile strength, material consumption, and build time through multi-objective optimization. Numerous studies [32–35] used Taguchi-based optimization in conjunction with numerical methods to analyse non-Newtonian and nanofluid flows by incorporating various effects like radiation, magnetic fields, and chemical effects.

This study aims to:

- Investigate steady, incompressible flow and thermal transfer of tricalcium phosphate ($\text{Ca}_3(\text{PO}_4)_2$)–molybdenum disulfide (MoS_2)/water hybrid nanofluid over a porous extending sheet.
- Incorporate the Hall current effect under strong magnetic fields into the governing equations, capturing realistic charge transport alterations typically neglected in classical magnetohydrodynamic nanofluid studies.
- Rigorously compare the thermal performance of $\text{Ca}_3(\text{PO}_4)_2$ – MoS_2 /water hybrid nanofluid against its mononanofluid counterpart, quantifying the heat transfer enhancement from dual nanoparticle synergy.
- Apply the Taguchi technique to evaluate the significance of key non-dimensional parameters and identify optimal conditions for maximum heat transfer, connecting mathematical modeling to practical engineering design.

In accordance with the objectives outlined, this research offers the following contributions to the existing body of knowledge. The use of $\text{Ca}_3(\text{PO}_4)_2$ – MoS_2 /water as a hybrid nanofluid is itself a distinctive and uncommon choice that separates this work from the mainstream literature. Building upon this, the study uniquely couples Hall current effects with hybrid nanofluid dynamics over a porous extending sheet, a combination rarely attempted before. Further novelty lies in the concurrent treatment of thermal radiation alongside a non-uniform heat source, reflecting far more realistic thermal conditions than those typically assumed. Most remarkably, the deliberate integration of the Taguchi

optimization methodology into this multi-physics nanofluid framework transforms the study from a purely theoretical exercise into a practically actionable engineering tool, making this work both scientifically rigorous and industrially meaningful.

2 Mathematical Formulation

This study investigates the continuous flow of an incompressible hybrid nanofluid near an upward porous extending sheet at the xz -plane in the presence of Hall current effects and an electric field (Figure 1). The sheet is stretched linearly in both positive and negative directions when two opposite and equal forces are assumed to act next to the x -axis while the origin remains constant. The research takes into account a non-Newtonian hybrid nanofluid that generates or absorbs heat and has electrical conductivity. The hybrid nanofluid contains $\text{Ca}_3(\text{PO}_4)_2$ and MoS_2 nanoparticles in addition to water as the base fluid. To account for the Hall current effect, high-frequency electron collisions are taken into consideration, and an electric field is supposed to be applied across the z -axis. A strong magnetic flux density B_0 is used to introduce the Hall effect, and a low magnetic Reynolds number is assumed to discard the generated magnetic field. Additionally, it is assumed that there are no changes in heat transfer or velocity along the z -axis, which is supported by taking into account an infinitely wide sheet.

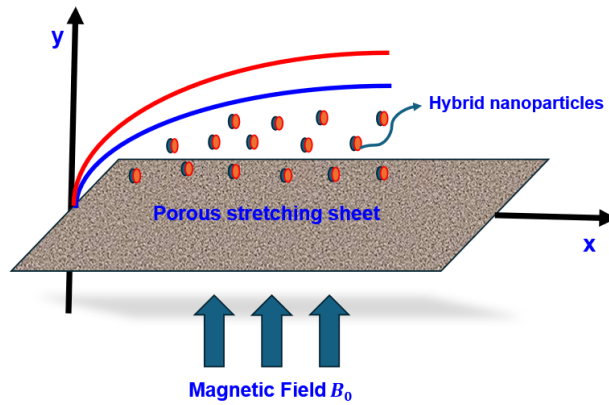


Figure 1. Flow configuration

The magnetic field follows the simplified version of Ohm's law below when the magnetic field is strong.

$$J = \sigma(E + q \times B)$$

where, $\sigma = \frac{e^2 n_e t_e}{m_e}$ is the electrical conductivity, n_e is the electron number density, m_e is the electron mass, and e is the electron charge. In addition, the current density vector is given by $J = (j_x j_y j_z)$, and the current can also be expressed using the relation: $j = \sigma \times (E + V \times B)$, where $B = (0, 0, 0)$ and the fluid velocity vector is $V = (u, v, w)$. The Hall parameter is defined as $m = \frac{\sigma B_0}{en_e}$. Using the aforementioned assumptions, the standardized Ohm's law for weakly ionized gases yields ($J_y = 0$) in the flow field. Thus, the elements of current density j_x and j_z are determined as:

$$j_x = \sigma \frac{B_0^2}{1 + m^2} (u + mw) \text{ and } j_z = \sigma \frac{B_0^2}{1 + m^2} (mu - w)$$

Since the Rosseland approach takes into consideration both self-absorption and emission as important elements impacting heat transmission, it is appropriate for predicting the radiative flux vector qr in dense fluids. The Rosseland approximation [36] applies because the absorption coefficient is usually significant and changes with wavelength. The governing equations representing the flow problem are as follows:

$$\frac{\partial u}{\partial x} + \frac{\partial v}{\partial y} = 0 \quad (1)$$

$$u \frac{\partial u}{\partial x} + v \frac{\partial u}{\partial y} = \frac{\mu_{\text{hnf}}}{\rho_{\text{hnf}}} \frac{\partial^2 u}{\partial y^2} - \frac{\sigma_{\text{hnf}}}{\rho_{\text{hnf}}} \frac{B_0^2}{1 + m^2} (u + mw) - \frac{\mu_{\text{hnf}}}{\rho_{\text{hnf}}} \frac{u}{k_p^*} \quad (2)$$

$$u \frac{\partial w}{\partial x} + v \frac{\partial w}{\partial y} = \frac{\mu_{\text{hnf}}}{\rho_{\text{hnf}}} \frac{\partial^2 w}{\partial y^2} + \frac{\sigma_{\text{hnf}}}{\rho_{\text{hnf}}} \frac{B_0^2}{1 + m^2} (mu - w) - \frac{\mu_{\text{hnf}}}{\rho_{\text{hnf}}} \frac{w}{k_p^*} \quad (3)$$

$$u \frac{\partial T}{\partial x} + v \frac{\partial T}{\partial y} = \frac{1}{(\rho C_p)_{\text{hnf}}} \left(\kappa_{\text{hnf}} + \frac{16\sigma^* T_\infty^3}{3k^*} \right) \frac{\partial^2 T}{\partial y^2} + \frac{\kappa_{\text{hnf}}}{(\rho C_p)_{\text{hnf}}} \frac{u_w}{\nu_f x} [\alpha^*(T_w - T_\infty) + (T - T_\infty)\beta^*] \quad (4)$$

The boundary conditions are as follows:

$$\left. \begin{aligned} v = 0, \quad u = ax, \quad w = 0, \quad T = T_w \quad \text{at } y = 0, \\ u \rightarrow 0, \quad w \rightarrow 0, \quad T \rightarrow T_\infty \quad \text{as } y \rightarrow \infty \end{aligned} \right\} \quad (5)$$

Similarity transformations are as follows:

$$\eta = y \sqrt{\frac{a}{\nu_f}}, u = axf'(\eta), v = -\sqrt{a\nu_f} f(\eta), w = axg(\eta), \theta = \frac{T - T_\infty}{T_w - T_\infty} \quad (6)$$

Eqs. (1)–(5) that control the system can be converted to the following expressions:

$$\frac{\frac{\mu_{\text{hnf}}}{\rho_f} f'''}{\rho_f} - f'^2 + f f'' - \frac{\frac{\sigma_{\text{hnf}}}{\rho_f} \text{Ha}}{1 + m^2} (f' + mg) - \frac{\frac{\mu_{\text{hnf}}}{\rho_f} K_p f'}{\rho_f} = 0 \quad (7)$$

$$\frac{\frac{\mu_{\text{hnf}}}{\rho_f} g''}{\rho_f} - f'g + f g' + \frac{\frac{\sigma_{\text{hnf}}}{\rho_f} \text{Ha}}{1 + m^2} (mf' - g) - \frac{\frac{\mu_{\text{hnf}}}{\rho_f} K_p g}{\rho_f} = 0 \quad (8)$$

$$\frac{1}{(\rho C_p)_f} \left(\frac{\kappa_{\text{hnf}}}{\kappa_f} + \text{Rd} \right) \theta'' + \frac{\frac{\kappa_{\text{hnf}}}{\rho_f}}{(\rho C_p)_f} [\alpha^* f' + \theta \beta^*] + \text{Pr} f \theta' = 0 \quad (9)$$

The transformed boundary conditions are as follows:

$$\left. \begin{aligned} f(\eta) = g(\eta) = 0, \quad f'(\eta) = 1, \quad \theta(\eta) = 1 \quad \text{at } \eta = 0, \\ f'(\eta) = g(\eta) = \theta(\eta) = 0 \quad \text{as } \eta \rightarrow \infty. \end{aligned} \right\} \quad (10)$$

The important dimensionless parameters are as follows:

$$MF = \frac{\sigma_f B_0^2}{\rho_f a}, \quad K = \frac{v_f}{k_p^* a}, \quad \text{Pr} = \frac{\kappa_f}{(\rho C_p)_f v_f}, \quad \text{Rd} = \frac{16\sigma^* T_\infty^3}{3\kappa_f k^*}$$

$$\frac{\mu_{\text{hnf}}}{\mu_f} = \frac{1}{(1 - \Phi_1)^{2.5} (1 - \Phi_2)^{2.5}} \quad (11)$$

$$\frac{\sigma_{\text{hnf}}}{\sigma_f} = \left\{ 1 + \frac{3 \left(\frac{\Phi_1 \sigma_{s1} + \Phi_2 \sigma_{s2}}{\sigma_f} - (\Phi_1 + \Phi_2) \right)}{2 + \left(\frac{\Phi_1 \sigma_{s1} + \Phi_2 \sigma_{s2}}{\sigma_f (\Phi_1 + \Phi_2)} \right) - \left(\frac{\Phi_1 \sigma_{s1} + \Phi_2 \sigma_{s2}}{\sigma_f} - (\Phi_1 + \Phi_2) \right)} \right\} \quad (12)$$

$$\frac{\rho_{\text{hnf}}}{\rho_f} = \left\{ (1 - \Phi_2) \left[1 - \Phi_1 + \Phi_1 \frac{\rho_{s1}}{\rho_f} \right] + \Phi_2 \frac{\rho_{s2}}{\rho_f} \right\} \quad (13)$$

$$\frac{(\rho C_p)_{\text{hnf}}}{(\rho C_p)_f} = \left\{ (1 - \Phi_2) \left[1 - \Phi_1 + \Phi_1 \frac{(\rho C_p)_{s1}}{(\rho C_p)_f} \right] + \Phi_2 \frac{(\rho C_p)_{s2}}{(\rho C_p)_f} \right\} \quad (14)$$

$$\frac{\kappa_{\text{hnf}}}{\kappa_{nf}} = \frac{\kappa_{s2} + 2\kappa_{nf} - 2\Phi_2 (\kappa_{nf} - \kappa_{s2})}{\kappa_{s2} + 2\kappa_{nf} + 2\Phi_2 (\kappa_{nf} - \kappa_{s2})}, \quad \frac{\kappa_{nf}}{\kappa_f} = \frac{\kappa_{s1} + 2\kappa_f - 2\Phi_1 (\kappa_f - \kappa_{s1})}{\kappa_{s1} + 2\kappa_f + 2\Phi_1 (\kappa_f - \kappa_{s1})} \quad (15)$$

The crucial physical characteristics of heat transmission rate and drag force can be expressed as:

$$Cf_x = \frac{\mu_{\text{hnf}} \left. \frac{\partial u}{\partial y} \right|_{y=0}}{\rho_f u_w^2}, \quad Cf_z = \frac{\mu_{\text{hnf}} \left. \frac{\partial w}{\partial y} \right|_{y=0}}{\rho_f u_w^2}, \quad Nu_x = \frac{-x \kappa_{\text{hnf}} \left. \frac{\partial T}{\partial y} \right|_{y=0} + q_r|_{y=0}}{\kappa_f (T_w - T_\infty)}.$$

The non-dimensional forms of these physical quantities using Eq. (5) are as follows:

$$\left. \begin{aligned} Cf_x \sqrt{Re_x} &= \frac{\mu_{\text{hnf}}}{\mu_f} f''(0), \\ Cf_z \sqrt{Re_x} &= \frac{\mu_{\text{hnf}}}{\mu_f} g'(0), \\ Nu_x \sqrt{Re_x^{-1}} &= - \left(\frac{\kappa_{\text{hnf}}}{\kappa_f} + Rd \right) \theta'(0) \end{aligned} \right\} \quad (16)$$

where, $Re_x^2 = \frac{x u_w}{\nu}$.

3 Methodology

This study employs a fourth-order Runge–Kutta method with a shooting strategy to address this problem numerically, focusing on a system of intricate equations. This method yields a sophisticated mathematical system characterized by high precision. The simulations transform the higher-order issue into a set of first-order equations: $f = \vartheta_1, f' = \vartheta_2, f'' = \vartheta_3, g = \vartheta_4, g' = \vartheta_5, \theta = \vartheta_6, \theta' = \vartheta_7$.

The transformed equations are as follows:

$$f''' = \frac{(\vartheta_2)^2 - (\vartheta_1)(\vartheta_3) + \frac{\sigma_{\text{hnf}}}{\rho_{\text{hnf}}} \frac{Ha}{1+m^2} ((\vartheta_2) + m(\vartheta_4)) + \frac{\mu_{\text{hnf}}}{\rho_f} K_p(\vartheta_2)}{\frac{\mu_{\text{hnf}}}{\rho_f} \frac{\mu_f}{\rho_{\text{hnf}}}}$$

$$g'' = \frac{(\vartheta_2)(\vartheta_4) - (\vartheta_1)(\vartheta_5) - \frac{\sigma_{\text{hnf}}}{\rho_{\text{hnf}}} \frac{Ha}{1+m^2} (m(\vartheta_2) - (\vartheta_4)) + \frac{\mu_{\text{hnf}}}{\rho_{\text{hnf}}} K_p(\vartheta_4)}{\frac{\mu_{\text{hnf}}}{\rho_f} \frac{\mu_f}{\rho_{\text{hnf}}}}$$

$$\theta'' = \frac{\frac{\kappa_{\text{hnf}}}{(\rho C_p)_{\text{hnf}}} [\alpha^*(\vartheta_2) + (\vartheta_6) \beta^*] - Pr(\vartheta_1)(\vartheta_7)}{\frac{\left(\frac{\kappa_{\text{hnf}}}{\kappa_f} + Rd \right)}{\frac{(\rho C_p)_{\text{hnf}}}{(\rho C_p)_f}}}$$

Transformed boundary conditions are as follows:

$$\begin{aligned} (\vartheta_1)(\eta) = (\vartheta_4)(\eta) = 0, (\vartheta_2)(\eta) = 1, (\vartheta_6)(\eta) = 1 \text{ at } \eta = 0 \\ (\vartheta_2)(\eta) = (\vartheta_4)(\eta) = (\vartheta_6)(\eta) = 0 \text{ as } \eta \rightarrow \infty \end{aligned}$$

The required solution necessitates an initial estimate using the boundary value problem solver `bvp4c` in MATLAB, which satisfies the prescribed boundary conditions. The value of η , originally defined as ∞ , is designated as $\eta = 7$ to meet software requirements.

4 Discussion of Results

This section explores the transport properties of a hybrid nanofluid by analyzing the influence of critical governing factors on momentum and temperature in an extending sheet configuration. The flow problem is formally represented by partial differential equations and, with the assistance of similarity variables, converted into ordinary differential equations. The fourth-order Runge–Kutta method is employed for the numerical solution of the ordinary differential equations. The influence of the Hall effect, thermal radiation, porosity effect and non-uniform heat source is taken into account. The Taguchi method is employed to optimize the thermal transfer rate. Table 1 describes the thermophysical properties of hybrid nanofluids.

Table 1. Properties of hybrid nanofluid [37, 38]

Nanofluid/Nanoparticle	C_p (kg ⁻¹ K ⁻¹)	ρ (kg m ⁻³)	σ (Ωm) ⁻¹	κ (W m ⁻¹ K ⁻¹)
Water	4179	997.1	5.5×10^{-6}	0.613
Tricalcium phosphate (Ca ₃ (PO ₄) ₂) (Φ_1)	842	3004	1×10^{-9}	1.5
Molybdenum disulfide (MoS ₂) (Φ_2)	397.7	5060	2.09×10^4	34.5

Table 2. Validation of $-\theta'(0)$ for different Prandtl numbers when $Rd = \alpha^* = \beta^* = \Phi_1 = \Phi_2 = 0$

Pr	Ref. [39]	Ref. [40]	Present Study
1.0	1.3333	1.3333	1.33333333
5.0	2.3801	2.3800	2.38013245
10	4.7968	4.7969	4.79695532

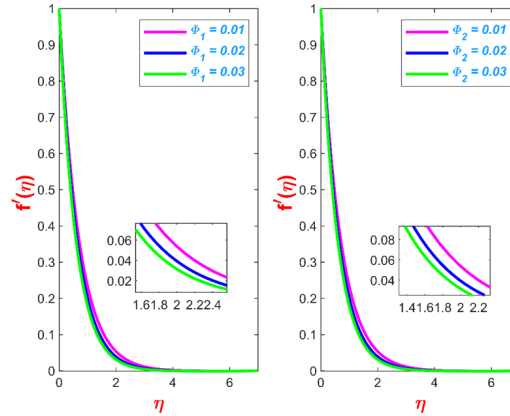


Figure 2. Impact of Φ_1 and Φ_2 on $f'(\eta)$

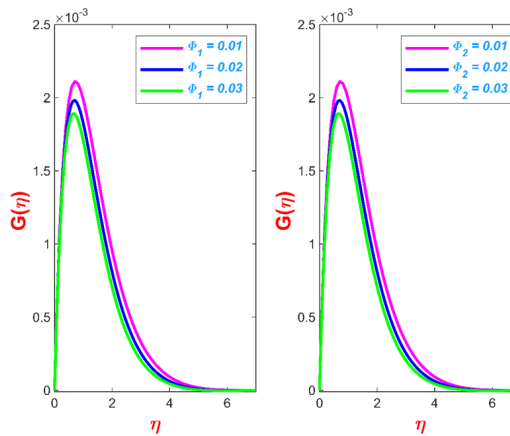


Figure 3. Impact of Φ_1 and Φ_2 on $g(\eta)$

Table 2 shows the validation of this research with previous studies. The incorporation of particle concentrations plays an essential role in the flow profiles. The concentration of the nanoparticle ($\text{Ca}_3(\text{PO}_4)_2$) is designated as Φ_1 , while the concentration of the MoS_2 particle is denoted as Φ_2 . The significance of the factors arises from the examination of the thermophysical models relevant to flow processes, with each model of density, viscosity, thermal conductivity, etc., depending upon the variations in volume fraction. Particle concentration, also referred to as volume fraction, denotes the percentage of particles present in the total volume of the liquid. Specifically, Figure 2 and Figure 3 illustrate the fluctuation of the concentrations Φ_1 and Φ_2 across the flow profiles, respectively. In both figures, the concentration range is limited to 2%, specifically $0 < \Phi_1, \Phi_2 < 0.03$. The graphical representation of these figures demonstrates that as Φ_1 and Φ_2 increase, both $f'(\eta)$ and $g(\eta)$ decrease. The dominance of the bi-hybrid nanofluid's density diminishes momentum, while an increase in conductivity leads to a retardation of the profile.

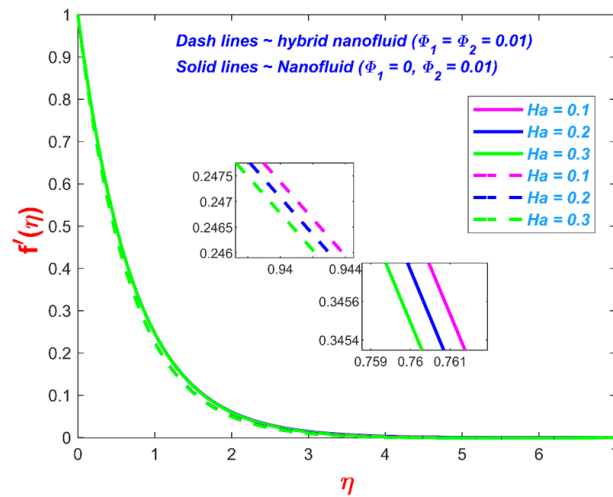


Figure 4. Impact of Ha on $f'(\eta)$

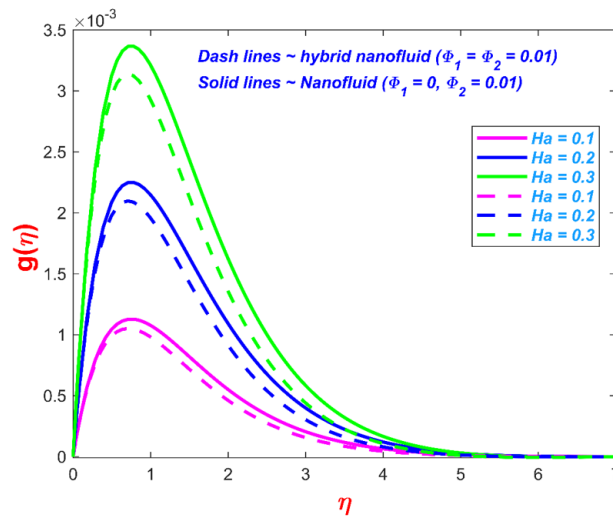


Figure 5. Impact of Ha on $g(\eta)$

The influence of Ha on $f'(\eta)$ and $g(\eta)$ is demonstrated in Figure 4 and Figure 5. The increasing values of Ha decreases $f'(\eta)$ whereas the opposite behavior is observed for $g(\eta)$. The cross-flow velocity is absent when the Hall current value is zero, correlating with Figure 6 which shows no cross-flow velocity when there is no magnetic field present. The physical interpretation of this result is that the magnetic field exerts a force on the moving charge carriers, thereby contributing to the induction of the Hall current. The Hall effect becomes significant when the magnetic field intensity is adequate. An extra potential difference is generated, resulting in an induced current that flows perpendicularly to the direction of the current as well as in the direction of the magnetic field. The variation of m with $f'(\eta)$ and $g(\eta)$ is visualized in Figure 6 and Figure 7. The increasing values of m decreases $f'(\eta)$ and the opposite behavior is observed for $g(\eta)$.

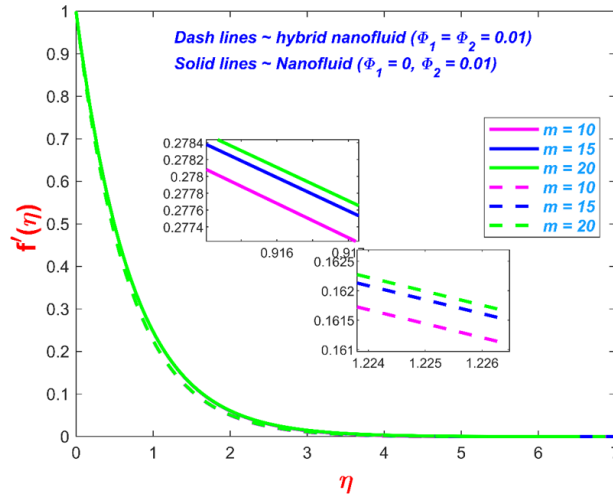


Figure 6. Impact of m on $f'(\eta)$

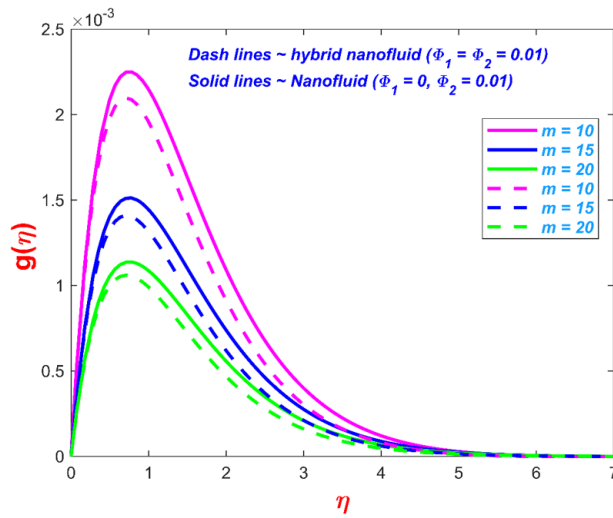


Figure 7. Impact of m on $g(\eta)$

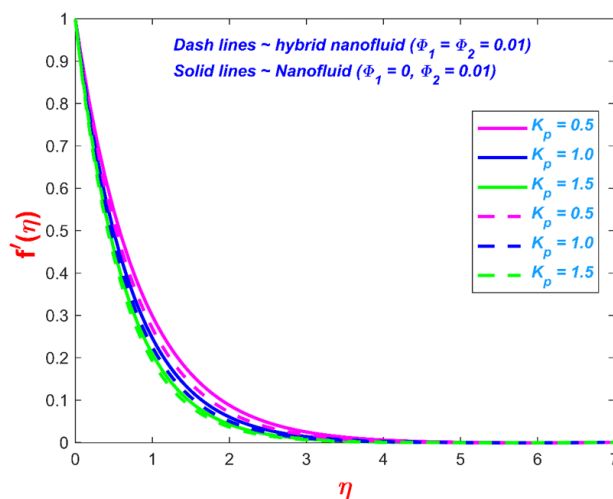


Figure 8. Impact of K_p on $f'(\eta)$

Figure 8 and Figure 9 display the significant consequences of permeability on $f'(\eta)$ and $g(\eta)$. The factor's distribution is depicted within a broad range of $0.5 < K_p < 1.5$. In this context, K_p denotes the behavior of the

flow profile as the fluid traverses a transparent fluid substrate, whereas the variation illustrates the flow through a porous substrate. The medium's resistivity tends to diminish the velocity profile in both axial and transverse directions, resulting in layer thinning. The negligible variance arises from the restricted range selection for the factor; however, the findings are illustrated with an enlarged view to clarify the differences between the profiles. The effect of permeability on temperature distribution is inverse, as fluid temperature increases with increased permeability. When the fluid velocity diminishes along the profile, the fluid produces energy at the surface's base, resulting in a considerable increase in temperature due to the accumulated energy.

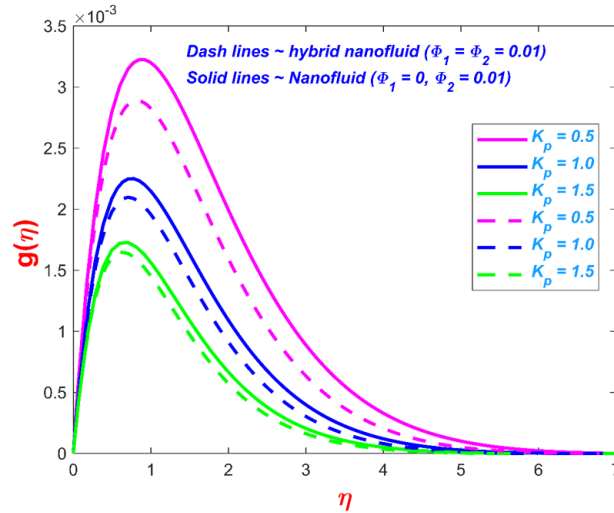


Figure 9. Impact of K_p on $g(\eta)$

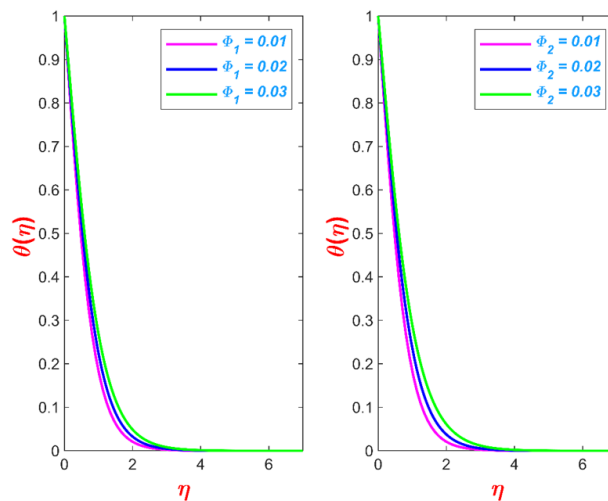


Figure 10. Impact of Φ_1 and Φ_2 on $\theta(\eta)$

Figure 10 examines the influence of solid nanoparticles Φ_1 and Φ_2 on the distribution of fluid temperature. The concentration of particles is a critical element that profoundly affects the thermal characteristics of nanofluids and hybrid nanofluids. The precise number of particles distributed within the base fluid is termed volume concentration. The solid volume concentrations significantly influence the increase in fluid temperature for the recommended values of the constructive factors.

The variation of time-dependent (α^*) and space-dependent (β^*) heat source parameters with $\theta(\eta)$ is demonstrated in Figure 11 and Figure 12. The increasing values of α^* and β^* intensifies $\theta(\eta)$. The incorporation of a non-uniform heat source elevates the surface temperature due to the accumulated energy at the surface. This stored energy induces movement toward the fluid region, which promotes an increase in fluid temperature, ensuring the exit temperature from the surface. This results in the cooling of the thermal boundary surface. The inclusion of additional nanoparticles in the base liquid of the hybrid nanofluid markedly enhances its thermal conductivity, resulting in a considerable rise in the fluid's temperature.

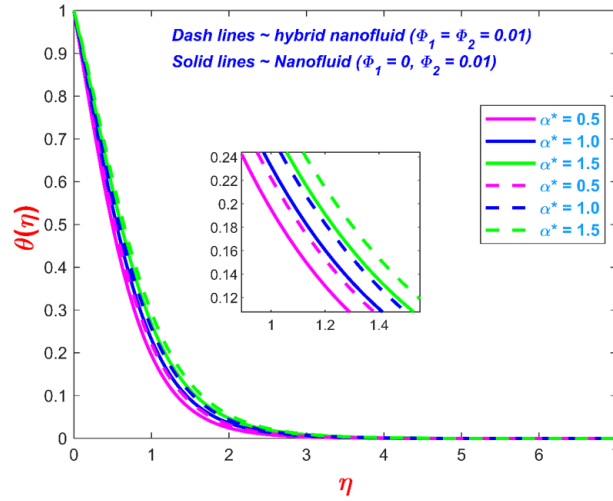


Figure 11. Impact of α^* on $\theta(\eta)$

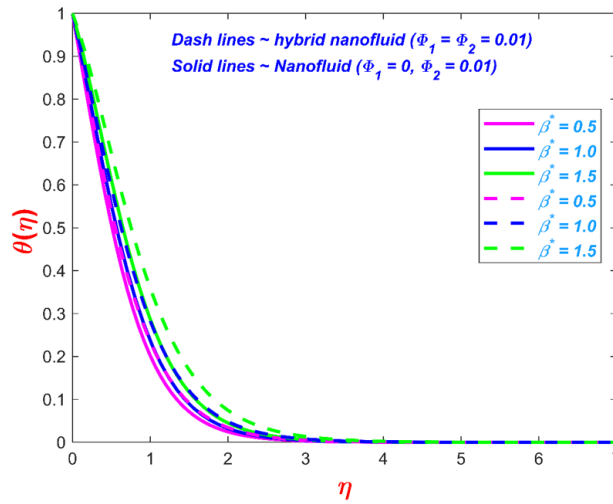


Figure 12. Impact of β^* on $\theta(\eta)$

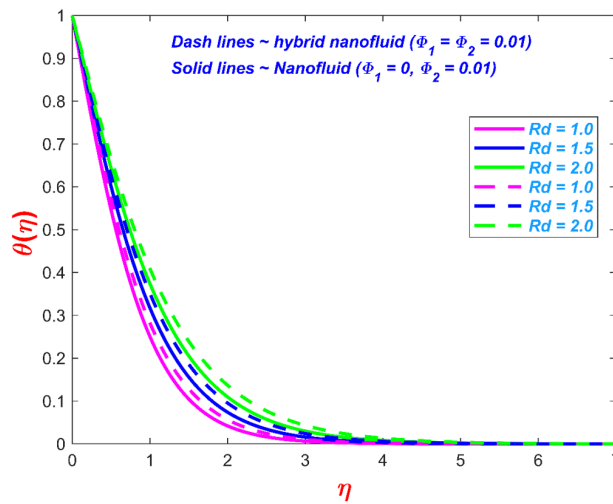


Figure 13. Impact of Rd on $\theta(\eta)$

The impact of Rd on the thermal profile is detailed in Figure 13. The quantity of electromagnetic waves that are transferred from the fluid element and subsequently transformed into thermal energy is commonly referred to as Rd .

It shows that the increased radiative heat significantly raises the fluid temperature because the radiating heat from the surface causes more energy to flow from the surface to the fluid medium. Furthermore, the enhanced thermal characteristics of the combined influence of the crystalline structure nanoparticles significantly increase the hybrid nanoparticles' considerable contribution compared to the nanofluid condition.

4.1 Interpretation of System Behavior for Engineering Design

The combined influence of Hall current, thermal radiation, porosity effect and non-uniform heat source provides a trade-off between axial and cross-flow velocities, crucial for efficient flow regulation. Growing values of Hall current amplifies cross-flow velocity, whereas permeability alters resistance and axial transport, offering prospects for enhanced system design. The augmentation of Φ_1 and Φ_2 significantly elevates thermal distribution due to the enhancement of thermal conductivity of nanoparticles in the system. The analysis indicates that increased radiation parameter values boost thermal profile, underscoring its significance in high-thermal environments. Collectively, these insights provide the practical guidance for improving and designing efficient advanced heat transfer systems.

5 Taguchi Method

Traditional computational design methods cannot handle complex computational problems, especially when there are many process elements. The traditional numerical method is excessively costly and complicated [26–28]. The Taguchi technique uses orthogonal arrays to reduce the number of computations while accounting for the whole parameter space. The minimization of experimental duration and expenses, together with the swift discovery of essential components, and the preservation of research resources are the primary advantages of using the Taguchi technique. As indicated in Table 3, the four primary parameters utilized in this investigation are the volume fraction, radiation parameter, and time- and space-dependent heat source parameters.

Table 3. Specification of control parameters and corresponding level settings

Input Parameters	Coded Value	First Level	Second Level	Third Level	Fourth Level
Φ_1	A	0.01	0.02	0.03	0.04
Rd	B	1.0	1.5	2.0	2.5
α^*	C	0.5	1.0	1.5	2.0
β^*	D	0.5	1.0	1.5	2.0

For this investigation, four elements and four levels are first determined. A complete factorial would require 256 trials. The Taguchi statistical technique recommends utilizing an L_{16} orthogonal array to maintain statistical coverage and balance, which may greatly minimize the amount of computational and experimental effort required. The L_{16} array for the Taguchi approach is shown in Table 4. Furthermore, Figure 14 represents the residual plot of Nu .

Table 4. L_{16} orthogonal array representing factor-level combinations

Runs	Φ_1	Rd	α^*	β^*	Nu	Signal-to-Noise Ratio
1	0.01	1.0	0.1	0.1	1.00264	0.0229
2	0.01	1.5	0.2	0.2	0.30290	-10.3740
3	0.01	2.0	0.3	0.3	0.72566	-2.7853
4	0.01	2.5	0.4	0.4	0.56561	-4.9497
5	0.02	1.0	0.2	0.3	0.88686	-1.0429
6	0.02	1.5	0.1	0.4	0.75812	-2.4052
7	0.02	2.0	0.4	0.1	0.68225	-3.3211
8	0.02	2.5	0.3	0.2	0.60651	-4.3432
9	0.03	1.0	0.3	0.4	0.79402	-2.0034
10	0.03	1.5	0.4	0.3	0.68422	-3.2961
11	0.03	2.0	0.1	0.2	0.64833	-3.7641
12	0.03	2.5	0.2	0.1	0.62338	-4.1049
13	0.04	1.0	0.4	0.2	0.79757	-1.9646
14	0.04	1.5	0.3	0.1	0.73711	-2.6494
15	0.04	2.0	0.2	0.4	0.57984	-4.7338
16	0.04	2.5	0.1	0.3	0.55981	-5.0392

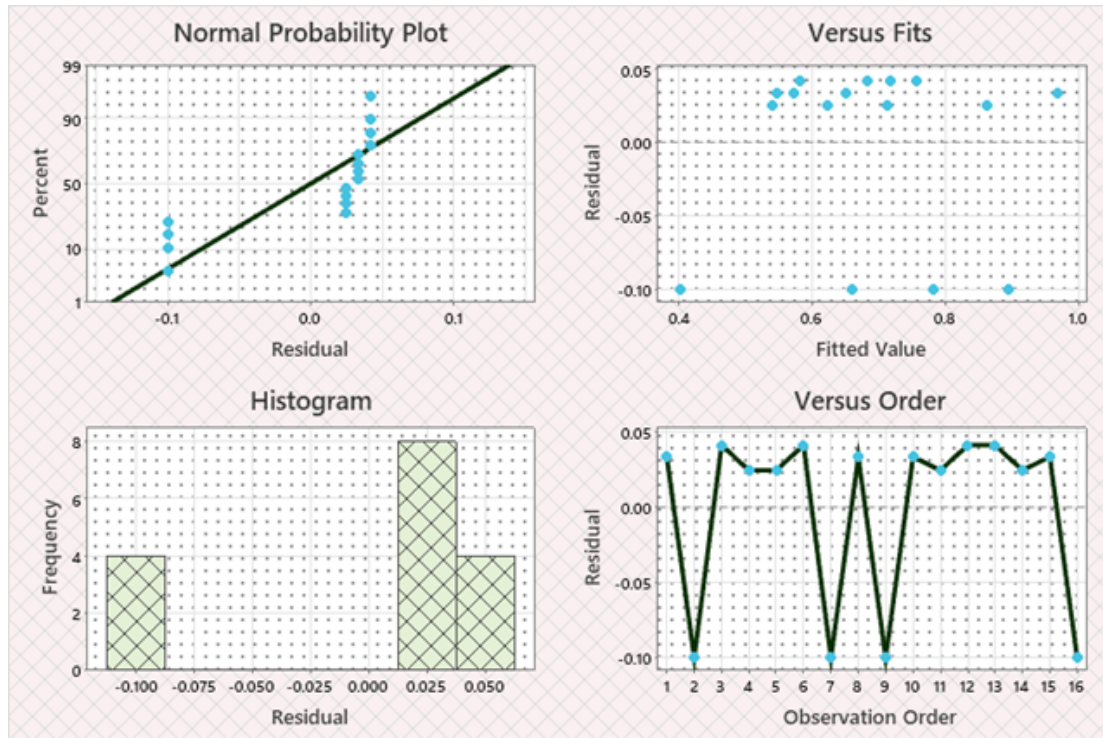


Figure 14. Residual plots for Nu

The equation below is employed to ascertain the minimal number of viable numerical runs.

$$N_Z = 1 + N_X(L - 1) \quad (17)$$

where, N_Z denotes the minimal quantity of calculations required, dictated by the number of control parameters (N_X) and levels (L). Four control features ($N_X = 4$) and four levels ($L = 4$) are considered. According to the aforementioned equation, a minimum of 13 numerical computations must be performed. For factors with three levels, the accessible orthogonal arrays are L_{16} , L_{32} , and alike formations. Therefore, the L_{16} orthogonal array is selected for the present work as it best matches the computational requirements and accommodates four levels for each parameter. The current study employs the “larger-the-better” criteria as its evaluative standard to achieve the goal of optimization of Nu .

$$\frac{S}{N} = -10 \log \left(\frac{1}{n} \sum \frac{1}{y^2} \right) \quad (18)$$

$$Nu = \begin{cases} 0.6847 - 0.0355A_{0.01} + 0.0488A_{0.02} + 0.0028A_{0.03} - 0.0161A_{0.04} + 0.1856B_1 \\ -0.0641B_{1.5} - 0.0257B_2 - 0.0958B_{2.5} + 0.0575C_{0.1} - 0.0864C_{0.2} + 0.0311C_{0.3} \\ -0.0023C_{0.4} + 0.0767D_{0.1} - 0.0958D_{0.2} + 0.0295D_{0.3} - 0.0103D_{0.4} \end{cases} \quad (19)$$

Table 5. ANOVA for Nu

Source	Adj SS	DF	Adj MS	F-Value	P-Value	% Contribution
A	0.01561	3	0.005204	0.29	0.832	4.17
B	0.19359	3	0.064531	3.60	0.161	51.73
C	0.04703	3	0.015677	0.87	0.543	12.57
D	0.06415	3	0.021385	1.19	0.444	17.15
Error	0.05382	3	0.017940			14.38
Total	0.37421	15				100

Note: ANOVA: analysis of variance

In order to make the required predictions and explain experimental data, analysis of variance (ANOVA) is utilized [29–32]. Table 5 shows the findings of the ANOVA on the Nusselt number. Table 6 displays the R-squared value of 85.62% and the adjusted R-squared value of 28.09%. The regression equation that ought to be applied to the model is as follows:

Table 6. R-squared values

Standard Error	R-squared	Predicted R-squared	Adjusted R-squared
0.133940	85.62%	0.00%	28.09%

6 Conclusion

This work examined the flow and thermal transmission properties of a water-based hybrid nanofluid over a porous extending sheet, considering the effects of Hall current, a non-uniform heat source, and thermal radiation. The dimensionless system of equations was numerically solved using the MATLAB *bvp4c* solver environment. Additionally, the Taguchi optimization method was utilized to identify ideal conditions for enhancing heat transfer efficiency in engineering applications. The main outcome of the present investigation is as follows:

- The $f'(\eta)$ profile is markedly affected by the resistive forces associated with the Hartmann number, while the $g(\eta)$ profile displays a contrasting pattern.
- Thermal radiation generates maximal intensity in heat transport phenomena at all regions.
- The thermal profile of the hybrid nanofluid demonstrates a more significant change than that of the traditional nanofluid.
- An R-squared value of 85.62% signifies that the dataset is robust and the model is considerable.
- The Taguchi-based L_{16} orthogonal array optimization indicates that Rd is the most influential parameter, contributing 51.73% to the heat transfer rate; therefore, it should be prioritized in system design and optimization.
- According to Taguchi optimization, engineers should primarily control Rd , followed by β^* and α^* , to maximize heat transfer efficiency in Hall-induced nanofluid systems.
- Hybrid nanomaterials enhance thermal performance and support efficient multiphysics system design.

Author Contributions

Conceptualization, R.P.S.; methodology, A.S.; software, A.S.; validation, S.P., V.V.K., and B.K.B.; investigation, A.S., S.P., V.V.K., and B.K.B.; writing—original draft preparation, A.S., S.P., V.V.K., and B.K.B.; writing—review and editing, R.P.S.; supervision, R.P.S. All authors have read and agreed to the published version of the manuscript.

Data Availability

Not applicable.

Acknowledgements

The authors Bimal Kumar Barik and Sriram Praharaj gratefully acknowledge the support provided by the Visvesvaraya PhD Scheme (Phase-II) of the Ministry of Electronics and Information Technology (MeitY), Government of India.

Conflicts of Interest

The authors declare no conflicts of interest.

References

- [1] B. K. Sharma, N. Poonam, and A. J. Chamkha, “Effects of heat transfer, body acceleration and hybrid nanoparticles (Au- Al_2O_3) on MHD blood flow through a curved artery with stenosis and aneurysm using hematocrit-dependent viscosity,” *Waves Random Complex Media*, vol. 35, pp. 11 842–11 872, 2022. <https://doi.org/10.1080/17455030.2022.2125597>
- [2] D. Mohanty, G. Mahanta, S. Shaw, and M. Das, “Thermosolutal Marangoni stagnation point GO– MoS_2 /water hybrid nanofluid over a stretching sheet with the inclined magnetic field,” *Int. J. Mod. Phys. B*, vol. 38, p. 2450024, 2024. <https://doi.org/10.1142/s0217979224500243>
- [3] C. Manimegalai and P. K. Kameswaran, “Impact of thermal radiation and magnetohydrodynamics on hybrid nanofluid flow over a vertical plate,” *Res. Eng.*, vol. 28, p. 106969, 2025. <https://doi.org/10.1016/j.rineng.2025.106969>
- [4] C. Parida, D. Mohanty, G. Mahanta, and S. Shaw, “Thermo-solutal impact of MHD hybrid nanofluid flow containing gyrotactic microorganisms over an inclined cylinder,” *Numer. Heat Transf. A Appl.*, vol. 87, pp. 1–27, 2025. <https://doi.org/10.1080/10407782.2025.2541813>
- [5] G. Yadav and R. Mehta, “Numerical analysis of MHD Darcy–Forchheimer Williamson hybrid nanofluid flow with brownian and thermophoretic effects,” *Discov. Appl. Sci.*, vol. 8, p. 420, 2026. <https://doi.org/10.1007/s42452-026-08241-9>

- [6] S. Praharaj and R. P. Sharma, "Hybrid analysis of deep learning and statistical approach in predicting heat transfer rate of radiative polar nanofluid flow with inertial drag," *Phys. Fluids*, vol. 38, p. 023604, 2026. <https://doi.org/10.1063/5.0305021>
- [7] A. Mishra, "Analysis of waste discharge concentration in radiative hybrid nanofluid flow over a stretching/shrinking sheet with chemical reaction," *Mech. Time Depend. Mater.*, vol. 29, p. 7, 2025. <https://doi.org/10.1007/s11043-024-09752-x>
- [8] P. Rana, B. Mahanthesh, K. Thriveni, and T. Muhammad, "Significance of aggregation of nanoparticles, activation energy, and Hall current to enhance the heat transfer phenomena in a nanofluid: A sensitivity analysis," *Waves Random Complex Media*, vol. 35, pp. 4820–4842, 2022. <https://doi.org/10.1080/17455030.2022.2065043>
- [9] A. K. A. Hakeem, S. Kirusakthika, B. Ganga, M. Akilesh, A. S. Dogonchi, and M. K. Nayak, "Hall current and non-linear slip impact on hydro-magneto-thermal hybrid nanofluid flow past a vertical rotating cone with sundry base fluids," *Numer. Heat Transf. A Appl.*, vol. 85, no. 14, pp. 2380–2395, 2023. <https://doi.org/10.1080/10407782.2023.2222904>
- [10] N. Kanimozhi, R. Vijayaragavan, B. R. Kumar, and A. J. Chamkha, "Investigation of Hall current and thermal diffusion effects on unsteady MHD mixed convective Jeffrey fluid flow over an inclined permeable surface with chemical reaction," *Eur. Phys. J. Plus*, vol. 139, p. 254, 2024. <https://doi.org/10.1140/epjp/s13360-024-05077-3>
- [11] K. Pratapa, S. Gollapalli, S. R. Sheri, M. Awais, H. A. Garalleh, and A. Al Agha, "Transient magnetohydrodynamic flow over a rotating vertical porous surface incorporating thermal radiation, hall and ion-slip effects: Using finite element method," *Results Chem.*, vol. 25, p. 103244, 2026. <https://doi.org/10.1016/j.rechem.2026.103244>
- [12] K. Varatharaj, R. Tamizharasi, R. Sivaraj, K. Vajravelu, and H. Thameem Basha, "Supervised machine learning analysis of Hall current and radiative effects in Casson nanofluid flow over a stretching surface with activation energy," *Int. J. Ambient Energy*, vol. 46, no. 1, p. 2549023, 2025. <https://doi.org/10.1080/01430750.2025.2549023>
- [13] S. A. Gaffar, O. A. Beg, and P. R. Reddy, "Simulation of magneto-convection nanofluid flow past a vertical semi-infinite plate with Hall current and ion-slip phenomena," *Can. J. Chem. Eng.*, 2026. <https://doi.org/10.1002/cjce.70382>
- [14] C. K. N. Bhargava, S. M. Ibrahim, and R. Kodi, "Effects of hall current, radiation absorption and diffusion thermo on an unsteady MHD flow of second grade fluid through porous media in the presence of joule heating and viscous dissipation," *Multiscale Multidiscip. Model. Exp. Des.*, vol. 8, p. 260, 2025. <https://doi.org/10.1007/s41939-025-00842-y>
- [15] V. R. Banakar, K. Karthik, S. P. Jena, and R. S. V. Kumar, "Optimizing and understanding complex relationships between micro-inertia and spin gradient viscosity in off-centered stagnation point flow," *Dyn. Atmos. Oceans*, vol. 114, p. 101660, 2026. <https://doi.org/10.1016/j.dynatmoce.2026.101660>
- [16] J. K. Madhukesh, S. O. Paramesh, G. D. Prasanna, B. C. Prasannakumara, M. I. Khan, S. Abdullaev, and G. Rasool, "Impact of magnetized nanoparticle aggregation over a Riga plate with thermal radiation in water- Al_2O_3 based nanofluid flow," *ZAMM–J. Appl. Math. Mech.*, vol. 106, no. 2, p. e202300270, 2026. <https://doi.org/10.1002/zamm.202300270>
- [17] J. Jayaprakash, V. Govindan, S. S. Santra, S. S. Askar, A. Foul, S. Nandi, and S. M. Hussain, "Thermal radiation, Soret and Dufour effects on MHD mixed convective Maxwell hybrid nanofluid flow under porous medium: A numerical study," *Int. J. Numer. Methods Heat Fluid Flow*, vol. 34, pp. 3924–3952, 2024. <https://doi.org/10.1108/hff-03-2024-0229>
- [18] A. Anjum, C. Maheswari, B. N. Lakshmi, R. M. Ramana, S. Peerusab, and S. A. Gaffar, "Computational study of magnetized 3D revolving hybrid nanofluid with non-linear thermal radiation and heat source/sink over a stretching sheet," *Multiscale Multidiscip. Model. Exp. Des.*, vol. 8, p. 200, 2025. <https://doi.org/10.1007/s41939-025-00748-9>
- [19] S. Sushma, C. G. Pavithra, K. J. Gowtham, and B. J. Gireesha, "Impact of similarity transformations on hybrid nanofluid thermal behavior with thermal radiation on nonlinear stretching surface via Hermite wavelet transformations," *Radiat. Eff. Defects Solids*, vol. 180, pp. 1077–1101, 2024. <https://doi.org/10.1080/10420150.2024.2436484>
- [20] T. Gupta, A. K. Pandey, and M. Kumar, "Comparative analysis of radiative heat transfer in CNT-based hybrid nanofluids over porous curved surface," *Chem. Eng. Sci.*, vol. 322, p. 123119, 2026. <https://doi.org/10.1016/j.ces.2025.123119>
- [21] N. A. Shah, K. Masood, M. D. Kumar, B. C. Prasannakumara, and G. Dharmiah, "Analysis of Von Karman transport considering Stefan blowing, isotropic slip and motile density: Adaptive neuro-fuzzy inference system and optimisation of particle swarms," *Eng. Appl. Artif. Intell.*, vol. 163, p. 113093, 2026. <https://doi.org/10.1>

- [22] B. Ramadevi, K. A. Kumar, V. Sugunamma, and N. Sandeep, "Influence of non-uniform heat source/sink on the three-dimensional magnetohydrodynamic Carreau fluid flow past a stretching surface with modified Fourier's law," *Pramana*, vol. 93, no. 6, p. 86, 2019. <https://doi.org/10.1007/s12043-019-1847-7>
- [23] K. Govindarajulu, A. Subramanyam Reddy, K. Jagadeshkumar, S. Srinivas, B. R. Kumar, and K. Vajravelu, "Entropy generation on MHD pulsatile flow of third grade hybrid nanofluid in a vertical porous channel with nonuniform heat source/sink, variable viscosity, thermal conductivity, and Joule heating: A numerical study," *Numer. Heat Transf. A Appl.*, vol. 85, no. 24, pp. 4184–4203, 2023. <https://doi.org/10.1080/10407782.2023.2255929>
- [24] J. K. Madhukesh, I. E. Sarris, K. Vinutha, B. C. Prasannakumara, and A. Abdulrahman, "Computational analysis of ternary nanofluid flow in a microchannel with nonuniform heat source/sink and waste discharge concentration," *Numer. Heat Transf. A Appl.*, vol. 85, no. 21, pp. 3665–3682, 2024. <https://doi.org/10.1080/10407782.2023.2240509>
- [25] A. Paul, J. M. Nath, and T. K. Das, "Thermally stratified Cu–Al₂O₃/water hybrid nanofluid flow with the impact of an inclined magnetic field, viscous dissipation and heat source/sink across a vertically stretching cylinder," *ZAMM–J. Appl. Math. Mech.*, vol. 104, p. e202300084, 2023. <https://doi.org/10.1002/zamm.202300084>
- [26] T. Grace, C. Maheswari, M. R. Ravuri, T. Anwar, B. N. Lakshmi, and S. M. Ibrahim, "Comparative analysis of impact of non-linear heat source on mixed convective chemically reacted MHD hybrid nanofluid/nanofluid/fluid over a stretched region," *Int. J. Thermofluids*, vol. 30, p. 101417, 2025. <https://doi.org/10.1016/j.ijft.2025.101417>
- [27] Monika, A. S. Negi, V. Kumar, and Shubhangi, "Comparative investigation of Darcy-Forchheimer MHD hybrid nanofluid (SWCNT–Al₂O₃, CNT–Al₂O₃/H₂O & MWCNT–CuO/H₂O) flow with heat source effect on a stretchable surface," *Int. J. Ambient Energy*, vol. 47, 2026. <https://doi.org/10.1080/01430750.2025.2588592>
- [28] S. Jagadha, D. Gopal, N. Patil, S. Singh, N. Kishan, and S. K. Abhilasha, "Effect of higher order chemical reaction and Joule heating on rotational and permeable radiative MHD flow of Casson manganese ferrite fluid with heat generation/absorption," *Multiscale Multidiscip. Model. Exp. Des.*, vol. 8, p. 164, 2025. <https://doi.org/10.1007/s41939-025-00756-9>
- [29] A. Sharma, A. Awasthi, T. Singh, R. Kumar, and R. Chauhan, "Experimental investigation and optimization of potential parameters of discrete V down baffled solar thermal collector using hybrid Taguchi-TOPSIS method," *Appl. Therm. Eng.*, vol. 209, p. 118250, 2022. <https://doi.org/10.1016/j.applthermaleng.2022.118250>
- [30] P. Kumar, F. Almeida, A. R. Ajakumar, and Q. Al-Mdallal, "Advancement of nanoparticles in blood flow with non-linear radiation and optimisation of irreversibility within the microchannel using analysis of variance and taguchi approach," *Int. J. Thermofluids*, vol. 24, p. 100975, 2024. <https://doi.org/10.1016/j.ijft.2024.100975>
- [31] U. I. Cicek and A. A. Johnson, "Multi-objective optimization of FDM process parameters for 3D-printed polycarbonate using Taguchi-based Gray Relational Analysis," *Int. J. Adv. Manuf. Technol.*, vol. 137, pp. 3709–3725, 2025. <https://doi.org/10.1007/s00170-025-15392-3>
- [32] P. Kumar, K. G. Vidhya, F. Almeida, and Q. Al-Mdallal, "Entropy optimization of inverse Darcy-Forchheimer model of Jeffrey fluid flow over a curved stretching surface using ANOVA-Taguchi technique," *Partial Differ. Equ. Appl. Math.*, vol. 14, p. 101183, 2025. <https://doi.org/10.1016/j.padiff.2025.101183>
- [33] A. Pandey and M. K. Mishra, "Optimizing thermal performance of nanofluid impinging upon a nonlinearly stretching sheet using Taguchi technique," *Numer. Heat Transf. A Appl.*, vol. 87, p. 2366444, 2024. <https://doi.org/10.1080/10407782.2024.2366444>
- [34] V. R. Banakar, R. N. Kumar, I. E. Sarris, and A. B. Sathisha, "Signal-to-noise ratio and ANOVA approach to analyze tetra-hybrid radiative nanofluid flow under horizontal magnetic field," *Int. J. Comput. Mater. Sci. Eng.*, p. 2650005, 2026. <https://doi.org/10.1142/s2047684126500053>
- [35] N. S. Asefa, K. Shahapurkar, T. Nigussie, A. A. Hassen, M. Elahi, Y. Fouad, I. Ali, S. Shelare, S. Sharma, V. K. B. Raja *et al.*, "Maximizing photovoltaic thermal system through computational fluid dynamics-driven multi-factor parametric optimization: A Taguchi-grey relational analysis method to enhancing electrical output and cooling efficiency for sustainable energy," *Case Stud. Therm. Eng.*, vol. 69, p. 105991, 2025. <https://doi.org/10.1016/j.csite.2025.105991>
- [36] A. K. Dash and S. R. Mishra, "Free convection of micropolar fluid over an infinite inclined moving porous plate," *J. Appl. Comput. Mech.*, vol. 8, no. 4, pp. 1154–1162, 2022. <https://doi.org/10.22055/JACM.2021.16703>
- [37] S. Rehman and A. Farooq, "Coupling physics-informed neural networks and regression techniques for modeling cubic stratified nanofluid flow in magnetic fields," *Chin. J. Phys.*, vol. 102, pp. 29–47, 2026. <https://doi.org/10.1016/j.cjph.2026.03.004>
- [38] R. P. Sharma, O. Prakash, S. R. Mishra, and P. S. Rao, "Hall current effect on molybdenum disulfide (MoS₂)-engine oil (EO) based MHD nanofluid flow in a moving plate," *Int. J. Ambient Energy*, vol. 43, no. 1, pp.

6201–6209, 2021. <https://doi.org/10.1080/01430750.2021.2003239>

- [39] F. Shahzad, D. Baleanu, W. Jamshed, K. S. Nisar, M. R. Eid, R. Safdar, and K. A. Ismail, “Flow and heat transport phenomenon for dynamics of Jeffrey nanofluid past stretchable sheet subject to Lorentz force and dissipation effects,” *Sci. Rep.*, vol. 11, p. 22924, 2021. <https://doi.org/10.1038/s41598-021-02212-3>
- [40] H. Waqas, U. Farooq, D. Liu, M. Abid, M. Imran, and T. Muhammad, “Heat transfer analysis of hybrid nanofluid flow with thermal radiation through a stretching sheet: A comparative study,” *Int. Commun. Heat Mass Transfer*, vol. 138, p. 106303, 2022. <https://doi.org/10.1016/j.icheatmasstransfer.2022.106303>